

HANDS-ON STUDY OF REDOX PROCESSES IN VANADIUM REDOX FLOW BATTERIES: A TEACHING MODULE FOR RENEWABLE ENERGY MASTER'S STUDENTS

BOGDAN CIPRIAN MITREA¹, MATEI TOM IACOB^{1*}, SANDA VOINEA¹, EDEN MAMUT^{2*}

¹ University of Bucharest, Faculty of Physics, Atomiştilor Street 405, 077125 Măgurele, Romania

² Ovidius Univ Constanta, 124 Mamaia Av, Constanta 900357, Romania

*Corresponding author: tom.iacob@3nanosae.org, eden.mamut@et-is.eu

Received

Abstract. The transition process from fossil-fuel-based energy systems to renewable energy sources is a critical step toward achieving climate neutrality. However, the intermittent nature of renewables such as solar and wind energy presents significant challenges for grid stability and energy storage. Vanadium redox flow batteries (VRFBs) offer a promising solution due to their ability to reversibly store chemical energy. This paper presents a hands-on teaching module designed for Master's students in renewable energy programs, focusing on the fundamental redox processes in VRFBs. The module includes the preparation of vanadium-based electrolyte solutions, electrochemical characterization via cyclic voltammetry, and performance evaluation through polarization tests. Results demonstrate the reversible redox behavior of V^{4+} species and provide insights into the practical operation of VRFBs. This educational approach not only reinforces theoretical knowledge but also equips students with practical skills essential for advancing energy storage technologies.

Key words: Vanadium redox flow batteries, electrochemistry, educational module.

1. INTRODUCTION

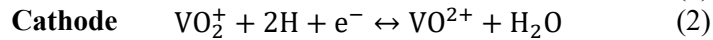
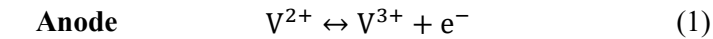
Given that the fossil-fuel-based energy sector accounts for approximately 40% of global anthropogenic CO₂ emissions, one of the foremost strategic imperatives for society is the transition towards renewable energy sources (e.g. wind, solar, hydroelectricity), concomitant with achieving climate neutrality by mid-century [1-2]. As the first steps in this process have been undertaken, the inherent limitations of these novel energy sources have also been identified and highlighted. Chief among these are the restricted capacity to supply a stable and continuous output of electricity — due to their dependence on variable meteorological conditions and locally available resources — and the substantial investments required to modernise existing infrastructure. One promising solution to these challenges lies in the implementation of vanadium redox flow battery (VRFB) technology.

In this context, the education and practical training of future specialists through targeted Master's programs in renewable energy is essential. Students should have access to interdisciplinary knowledge and hands-on experience required to develop, implement, and optimise advanced energy storage systems by understanding processes and technologies [3-5].

The objective is to develop a vanadium-ion-based battery in the form of a demonstrative model, enabling the study of oxidative states and the understanding of the electrochemical processes underlying the operation of such a device. The following sections review preliminary attempts at synthesising the electrolyte solution and assembling the battery, as well as the results obtained from electrochemical methods used to investigate reaction kinetics.

2. VANADIUM REDOX FLOW BATTERY: THEORETICAL AND TECHNOLOGICAL ASPECTS

As shown in Fig. 1, a typical VRFB cell includes several key components: the anode and cathode electrodes, an electrolyte solution, an ion exchange membrane, circulation pumps, and electrolyte reservoirs. The primary role of the membrane is to separate the two compartments of the cell whilst facilitating selective proton transport. Driven by pumps, V^{4+}/V^{5+} ion couples are supplied to the positively polarised compartment and V^{3+}/V^{2+} couples to the negatively polarised compartment, with both solutions prepared in sulfuric acid (H_2SO_4) [6]. The operating principle of VRFBs involves the reversible storage of chemical energy through the various accessible oxidation states of vanadium: V^{2+} , V^{3+} , V^{4+} , V^{5+} [7-9]. Electrons generated from electrochemical reactions are harvested through current collectors, which are electrically interfaced with a power supply or load. Due to the reversible nature of these reactions, the consumed ionic species can be regenerated during the charging cycle when an external potential is applied. The main electrode reactions occurring at the surfaces of the electrodes are:



Discharge \rightarrow \leftarrow Charge

The key electrochemical reactions occurring during the charging and discharging cycles of the redox flow battery [10]: The energy storage capacity of a VRFB is determined by the volume of the electrolyte and the concentration of vanadium ions, which in practice rarely exceeds $2 \text{ mol}\cdot\text{L}^{-1}$. However, structural imperfections in the ion-exchange membrane significantly impact the theoretical capacity by facilitating parasitic side reactions that impair battery performance:

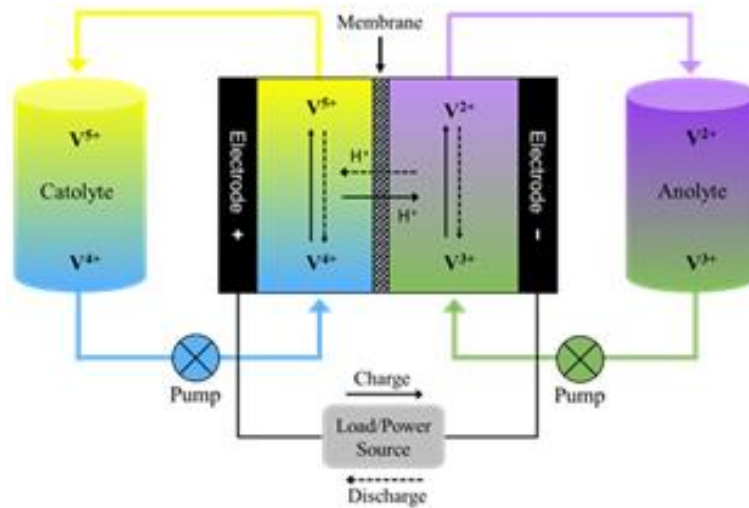
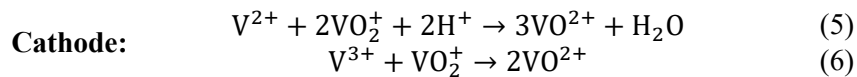
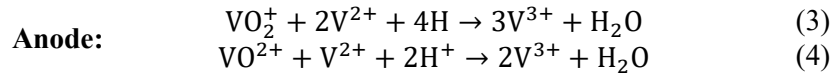


Fig. 1 – General scheme of a VRFB and its main reactions during charge/discharge cycles. The full color version may be accessed at <https://trp.nipne.ro>.

1) Vanadium ion crossover. Since the proton-exchange membrane is not perfectly selective, small amounts of vanadium ions permeate from the anolyte to the catholyte and vice versa, where they react instantaneously with the other ionic species present in the electrolyte [11-12]. The following examples illustrate these reactions:

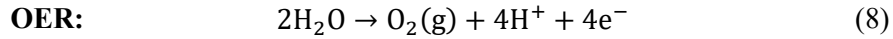
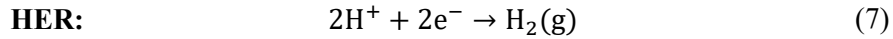


As the electrolyte flow is asymmetric, dilution and concentration of the electrolyte occur in the opposite compartments, ultimately resulting in self-discharge of the battery [4].

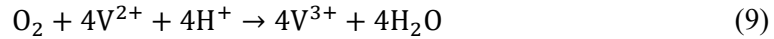
2) Water transport. In specific instances, water molecules migrate across the ionic membrane due to diffusive, osmotic, electro-osmotic forces or pressure gradients. Consequently, this leads to a change in the volume of the electrolyte solution [4].

3) Secondary gas-evolution reactions. As the electrolyte participates in the electron transfer process, gaseous products may form at the electrode surface, interfering with the vanadium redox reactions. During the charging process, at the anode, a portion of the current is consumed by protons, leading to the hydrogen

evolution reaction (HER). This phenomenon is responsible for slowing down the reduction of V^{3+} in the anolyte compared to the oxidation of V^{4+} in the catholyte. Specifically, the electrolyte enters a state of imbalance because the concentrations of ionic species in the two compartments become unequal—a factor that further contributes to the corrosion of the carbon electrodes and the bipolar plates. Conversely, at the cathode, the oxygen evolution reaction (OER) occurs less frequently and produces similar detrimental effects to those of HER [4]:



4) Air-oxidation. When the anolyte reservoir is exposed to air, atmospheric oxygen dissolves into the electrolyte, inducing the oxidation of V^{2+} to V^{3+} [13-14]. The corresponding chemical reaction is:



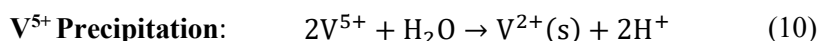
To prevent this phenomenon, periodic purging with N_2 and minimising the exposure of the anolyte reservoir to air are recommended [4].

5) Vanadium precipitation. The risk of vanadium ion precipitation increases with both concentration and thermal instability. This can lead to the clogging of electrolyte flow channels, damage to the ion-exchange membrane and, consequently, degradation of VRFB performance. Among the four ionic species, V^{5+} is the most unstable and tends to precipitate as V_2O_5 at temperatures exceeding 40°C . Conversely, at temperatures below 5°C , the other vanadium ions may precipitate as sulphates. For this reason, VRFBs are commonly operated within the temperature range of $5\text{--}40^\circ\text{C}$ [4].

6) Corrosion of solid components. Since the internal environment of VRFBs is highly corrosive due to the low pH of the electrolyte solution and the oxidative action of V^{3+} ions, carbon-based electrodes, bipolar plates, and chemically stable membrane are typically employed. However, despite these precautions, corrosion of various VRFB components has still been reported [15-16], especially under system overcharging. The effects of the processes outlined above are cumulative and generate, over successive charge–discharge cycles, a phenomenon known as electrolytic imbalance [4]. The chemical processes described in (1) and (2) are the primary cause of stoichiometric imbalance—a condition that can be remedied by remixing the electrolyte solutions from both reservoirs to equalise the vanadium ion concentrations. By contrast, the faradaic imbalance associated with processes (3) and (4) can be corrected through more complex electrochemical or chemical interventions. The key difference between these two forms of imbalance lies in the

fact that only in the latter case does the vanadium change its ionic state. In contrast, processes (5) and (6) rarely occur during typical VRFB operations; however, once detected, corrective measures must be implemented to address their underlying causes [4].

Research in the field of VRFBs has focused on resolving the aforementioned limitations, and, as a result, these types of batteries have been implemented on an industrial scale since the 1980s. VRFBs have emerged as a robust and commercially viable energy-storage technology, with a long-standing development history and proven installations worldwide. Since their inception in the 1980s, VRFBs have undergone significant advances and have gained prominence as a competitive energy-storage solution [17]. Key achievements include - Commercial success:



VRFBs have evolved from research projects into commercially successful technologies, with numerous companies manufacturing VRFB systems. Large-scale installations, including the 200 MW Rongke Power project in China, demonstrate the technology's scalability [18]. Energy density: VRFBs have a relatively low energy density (25–35 Wh/L) compared to lithium-ion batteries (LIBs), which typically achieve 250 Wh/L or more. However, VRFBs offer distinct advantages in terms of longevity. Longevity and durability: VRFBs are renowned for their exceptional lifespan, capable of delivering 12000 charge-discharge cycles. The use of the same metal (vanadium) in both electrolytes enables prolonged service life. Furthermore, vanadium is recyclable, contributing to the sustainability of this technology [19]. Commercial VRFBs typically operate at current densities of 80–100 mA/cm² and exhibit power densities of approximately 100 mW/cm². Ongoing research and development efforts aim to enhance efficiency and further increase power densities [20]. With response times on the order of milliseconds, VRFBs are well-suited to manage rapid fluctuations in grid power demand. They can thus become a key asset for grid support, especially during sudden network disturbances. Despite challenges, VRFBs are poised to play a vital role in the future of grid-scale energy storage.

3. EXPERIMENTAL METHODS

3.1 PREPARATION OF VANADIUM-BASED ELECTROLYTE SOLUTIONS

A 75ml solution of 6M H₂SO₄ was prepared. The mixture was heated to 90 °C using a hot plate and homogenised via magnetic stirring. Over 2–3 minutes, V₂O₅ was gradually added to the hot acid solution, maintaining continuous stirring

throughout. The temperature was held constant at 90 °C for 1 hour to ensure a complete reaction. Subsequently, the volume was adjusted to 200 mL with ultrapure water.

During the reduction process, a noticeable colour change was observed, corresponding to the successive changes in vanadium oxidation states. The initial yellow-orange hue, characteristic of V^{5+} , transitioned to dark green V^{3+} and finally to blue, indicating the presence of V^{4+} . Chemically, vanadium pentoxide undergoes reduction to the dioxovanadium ion in the presence of H_2SO_4 and water. Metallic zinc serves as the reducing agent, donating electrons and oxidising to Zn^{2+} . This facilitates the reduction of vanadium from the +5 to the +4 oxidation state. Protons supplied by the acid promote electron transfer and stabilisation of the reduced vanadium species.

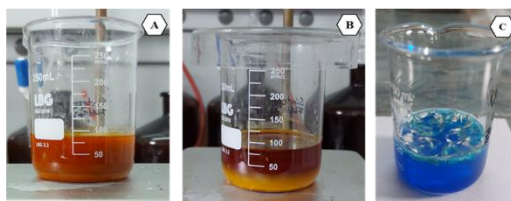
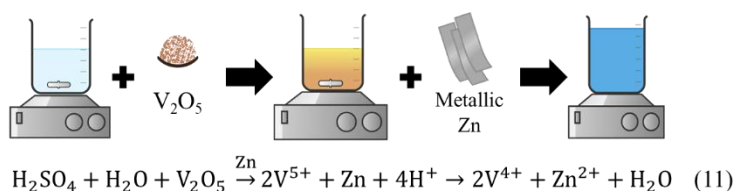
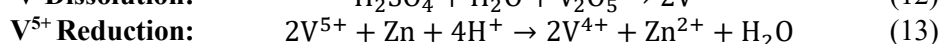
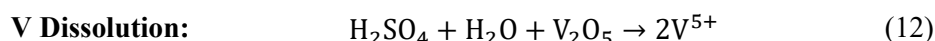


Fig. 2 – Preparation of V^{4+} electrolyte solution: (A) after adding V_2O_5 , (B) after heating to 90°C, and (C) after reduction to V^{4+} . The full color version may be accessed at <https://rrp.nipne.ro>.



In this procedure, the previously prepared V^{4+} solution was utilised as the anolyte in a VRFB with a total electrolyte volume of 30 mL. A 20 mL mixture was prepared, comprising 2 mL of V^{4+} solution, 16 mL of ultrapure water, and 2 mL of a MXene suspension (either V_2C or Ti_2C). The resulting dispersion was homogenised before use to ensure uniform distribution of the MXene nanosheets. This composite anolyte was then introduced into the anode compartment of the VRFB system for electrochemical evaluation.

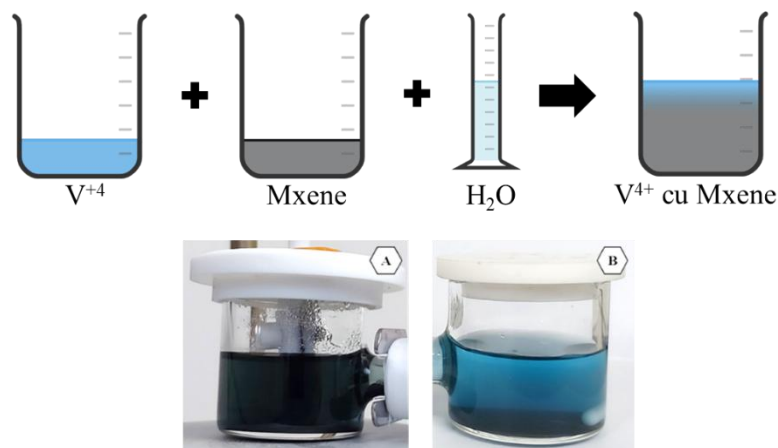


Fig. 3 – Schematic for preparing V^{4+} - MXene electrolyte solution as VRFB anolyte: (A) with TiC_2 MXene and (B) with V_2C MXene. The full color version may be accessed at <https://rrp.nipne.ro>.

3.2 CHARACTERISATION METHODS

Electrochemical characterisation of the electrolyte solutions and the VRFB was carried out using an OrigaFlex OGF500 electrochemical workstation (OrigaLys, France). Cyclic voltammetry (CV) measurements were performed in a single-chamber electrochemical cell with a total volume of 30 mL, configured in a three-electrode system. The working electrode (WE) and auxiliary electrode (AUX) consisted of non-teflonised carbon paper (1×1 cm, Ballard), while the reference electrode (RE) was Ag/AgCl (3 M KCl).

The parameters employed for the CV measurements were as follows: potential window of -1500 mV to $+1500$ mV, scan rate of $10 \text{ mV} \cdot \text{s}^{-1}$, maximum current of $+100$ mA, minimum current of -100 mA, and a total of 10 cycles. Charge-discharge tests and polarisation curve analyses were conducted in a dual-chamber cell configuration using a Nafion ion exchange membrane. Carbon electrodes were employed for both the working and auxiliary electrodes to investigate the redox processes undergone by V^{4+} at both the anode and cathode during the battery charging phase. The system was powered using a DC power supply (TTi, model PL601), applying a voltage in the range of 5–6 V and a current of approximately 15–20 mA. To prevent oxidation reactions caused by atmospheric oxygen, both compartments of the electrochemical cell were hermetically sealed.

4. RESULTS AND DISCUSSIONS

4.1. V⁴⁺ BASED BATTERY

The electrochemical profile of the vanadium redox couples, as revealed through CV, presents distinct peaks corresponding to the various oxidation and reduction transitions of vanadium species under acidic conditions. The anodic peak observed at -0.910 V is most likely attributed to the oxidation of V^{2+} to V^{3+} . This oxidation potential is considerably more negative than the standard potential of the V^{3+}/V^{2+} redox couple (-0.452 V vs. Ag/AgCl), indicating the presence of a substantial overpotential [21]. The corresponding cathodic peak for the reduction of V^{3+} to V^{2+} appears at -1.45 V, further deviating from the expected standard potential. This pronounced peak separation suggests slow electron transfer kinetics and the influence of the electrolyte composition—particularly the concentration of sulphuric acid and the presence of specific counter-ions—which likely contribute to the quasi-reversible nature of this redox pair [22].

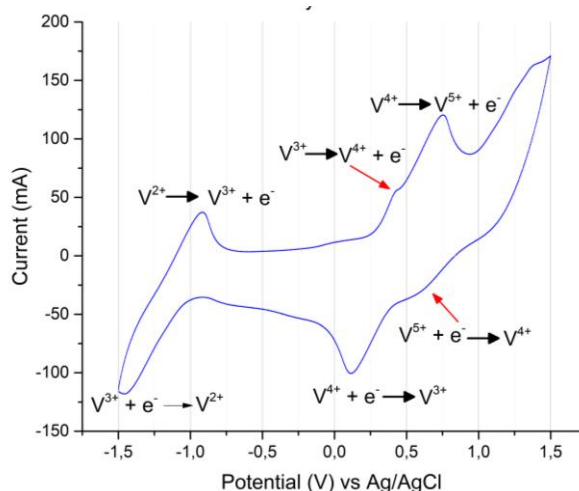


Fig. 4 – Cyclic voltammogram of V⁴⁺ electrolyte solution, scanned from -1.5 V to $+1.5$ V at 100 mV/s. The full color version may be accessed at <https://rrp.nipne.ro>.

The oxidation of V^{3+} to V^{4+} appears at 0.428 V, which is positively shifted from its standard potential of 0.140 V vs. Ag/AgCl. This shift may again indicate kinetic limitations or interfacial effects at the electrode-electrolyte interface. Conversely, the reduction of V^{4+} to V^{3+} is detected at 0.11 V, a value much closer to the standard potential [22], suggesting that the reduction process is kinetically more favourable. This asymmetry may be explained by the nature of the structural transformations involved: the oxidation process entails the formation of the oxovanadium ion V^{4+} , which likely requires higher activation energy due to bond

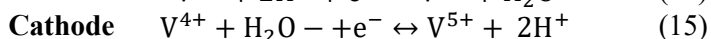
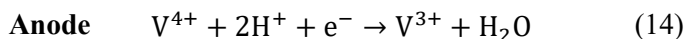
formation, whereas the reverse reaction—bond cleavage during reduction—proceeds more readily.

At higher potentials, the V^{4+}/V^{5+} couple is identified. The oxidation peak at 0.76 V corresponds to the transition from V^{4+} to V^{5+} [23], and is relatively close to the standard redox potential of 0.803 V vs. Ag/AgCl, indicating a near-reversible behaviour. The corresponding reduction peak, observed at 0.64 V, is also in proximity to the standard potential, and the relatively small overpotential suggests efficient electron transfer. Minor shifts in both anodic and cathodic peaks may be attributed to the proton activity and ionic strength of the acidic medium, factors known to affect the electrochemical response of vanadium species [24]. Finally, the anodic peak detected at 1.49 V is associated with the onset of the OER, which occurs when the potential exceeds the stability window of water. This parasitic process is characteristic of aqueous acidic systems at high anodic potentials and represents a limiting factor for the upper operational voltage of the electrochemical cell.



Fig. 5 – VRFB battery with carbon felt electrodes and V^{4+} electrolyte solution at a 2:10 dilution with ultrapure water, showing charging color stages: (A) initial blue V^{4+} anolyte and catholyte, (B) intermediate color transition, and (C) final green V^{3+} anolyte and yellow V^{5+} catholyte after 24 hours. The full color version may be accessed at <https://rrp.nipne.ro>.

Fig. 5 presents a chronological sequence of images captured during the experiment. (A) At the initial stage, the electrolyte solution in both compartments consists of V^{4+} . During the charging process, redox reactions occur at both the anode and cathode, as outlined below. These redox processes induce changes in the oxidation state of vanadium, which in turn result in visible colour changes in the electrolyte solutions. (B) After approximately 3–4 hours from the start of the experiment, partial oxidation of the catholyte becomes evident, as indicated by a colour transition from blue to green turquoise. Simultaneously, the anolyte shifts to a darker shade of blue, reflecting ongoing reduction. (C) After 24 hours, the electrochemical transformations are completed, with the catholyte fully oxidised to V^{5+} and the anolyte reduced to V^{3+} , as demonstrated by the final distinct colour changes.



The polarization curve in Fig. 6 for the base vanadium electrolyte battery exhibits an open circuit voltage (OCV) of approximately 1.3 V, consistent with the standard potential of the V^{2+}/V^{3+} and V^{4+}/V^{5+} redox couples in a typical VRFB electrolyte. At a current density of 0.036 mA/cm^2 , the voltage is $\sim 0.59 \text{ V}$, with a power density of $\sim 0.47 \text{ } \mu\text{W/cm}^2$, reflecting significant activation and ohmic losses, likely due to a large electrode surface area or low vanadium concentration reducing power density. At 0.059 mA/cm^2 , the voltage drops to $\sim 0.19 \text{ V}$, with a power density of $\sim 0.24 \text{ } \mu\text{W/cm}^2$, indicating severe polarization losses. The ohmic region ($0.003\text{--}0.036 \text{ mA/cm}^2$) shows a steep slope of $dV/dI \approx -16 \text{ V}/(\text{mA/cm}^2)$, corresponding to an area-specific resistance $R_o \approx 16 \text{ } \Omega \cdot \text{cm}^2$ and a low ionic conductivity. A pronounced voltage drop beyond 0.036 mA/cm^2 , reaching $\sim 0.0027 \text{ V}$ at 0.08 mA/cm^2 , indicates extreme concentration polarization, driven by mass transport limitations, likely due to diffusion constraints in the electrode. These results suggest that this configuration is unsuitable for practical VRFB applications due to its exceptionally low power output, likely resulting from a large electrode surface area distributing total power over a greater area.

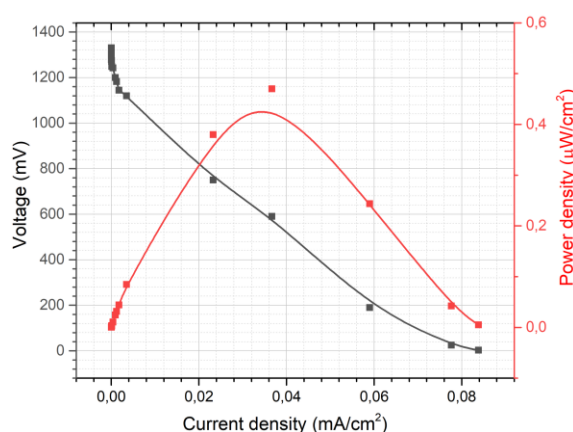


Fig. 6 – Polarization curve, derived from experimental discharge data, for a VRFB with V^{4+} electrolyte solution, showing a maximum power output of $700 \text{ } \mu\text{W}$. The full color version may be accessed at <https://rrp.nipne.ro>.

4.2 ELECTROLYTE SOLUTION: V^{4+} WITH MXENE – V_2C

In the voltammogram presented in Fig. 7, two principal redox couples can be identified: V^{5+}/V^{4+} and V^{3+}/V^{2+} . On the anodic sweep, a well-defined oxidation peak is observed at approximately $+0.75 \text{ V}$, corresponding to the oxidation of V^{4+} to V^{5+} . In addition, a broader and less intense peak appears in the range of $+0.8\text{--}0.9 \text{ V}$, which is likely associated with the oxidation of V^{2+} to V^{3+} . During the cathodic sweep, a clear reduction peak is detected at 0 V , indicative of the V^{5+} to V^{4+} transition. A

second cathodic peak appears at approximately -1.5 V, attributed to the reduction of V^{3+} to V^{2+} . The substantial separation between the anodic and cathodic peak potentials is noteworthy—approximately 750 mV for the V^{5+}/V^{4+} couple and over 2 V for the V^{3+}/V^{2+} couple. These deviations significantly exceed the theoretical value of 59 mV expected for a reversible one-electron transfer at 25 °C, suggesting that the redox processes are either irreversible or, at best, quasi-reversible in nature.

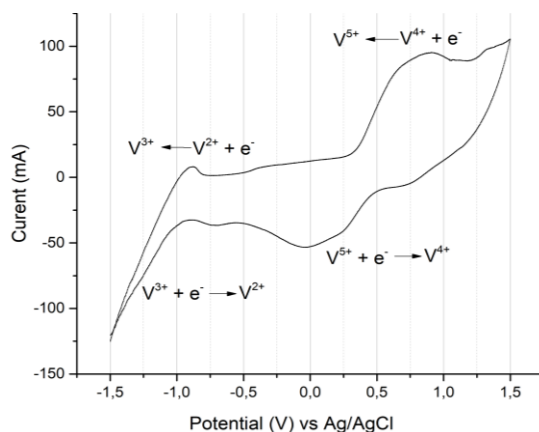


Fig. 7 – Cyclic voltammogram of V^{4+} - V_2C MXene electrolyte solution, scanned from -1.5 V to $+1.5$ V at 100 mV/s.

Such large peak separations are indicative of sluggish electron-transfer kinetics and may also imply the involvement of additional chemical steps following electron transfer. These mechanisms are characteristic of electron transfer followed by a chemical reaction or electron transfer–chemical reaction–electron transfer processes. This interpretation is consistent with previous reports in the literature, which describe similar electrochemical behaviour for vanadium species in aqueous media, where multivalent transitions are frequently coupled with proton exchange or changes in the coordination environment [25]. V_2C MXenes significantly contribute to the electrochemical response through several synergistic properties, including their large specific surface area, high electrical conductivity, interfacial redox activity, pseudocapacitive behaviour, and ion intercalation capability [26-27]. These characteristics may account for the broadening and asymmetry of the redox peaks, as well as the stabilisation of intermediate oxidation states of vanadium. Furthermore, interactions with surface functional groups ($-OH$, $-F$, $-O$), along with adsorption phenomena, may further influence the observed redox behaviour.



Fig. 8 – VRFB battery with V^{4+} - V_2C MXene electrolyte solution at a 1:9 dilution ratio (anolyte in right compartment), showing charging color stages: (A) initial blue V^{4+} anolyte and catholyte, (B) first visible V^{3+} reduction signs after 2 hours, and (C) final green V^{3+} anolyte and yellow V^{5+} catholyte after 24 hours. The full color version may be accessed at <https://rrp.nipne.ro>.

The polarization curve in Fig. 9 for the VRFB with the V_2C MXene - modified electrolyte displays a reduced OCV of approximately 1 V, suggesting possible side reactions or altered redox potentials due to the additive's interactions with vanadium ions or electrode surfaces. At a current density of 1.0 mA/cm^2 , the voltage is $\sim 0.664 \text{ V}$, creating a steeper voltage drop giving higher activation losses (increased by $\sim 20\%$ compared to standard VRFBs). At 2.0 mA/cm^2 , the voltage drops to $\sim 0.367 \text{ V}$ reflecting elevated ohmic losses. The maximum power density of 1 mW/cm^2 at 1.45 mA/cm^2 is significantly higher than the basic electrolyte's $\sim 0.47 \mu\text{W/cm}^2$, though lower than typical VRFB performance. The ohmic region ($0.5\text{--}1.5 \text{ mA/cm}^2$) exhibits a slope of $dV/dI \approx -0.333 \text{ V}/(\text{mA/cm}^2)$, corresponding to $R_o \approx 0.333 \Omega$. A sharp voltage drop beyond 1.5 mA/cm^2 , reaching $\sim 0.01 \text{ V}$ at 3.3 mA/cm^2 , indicates severe mass transport limitations. These characteristics imply that V_2C MXene addition compromises electrochemical performance compared to standard VRFBs but is significantly more effective than the basic electrolyte under these experimental conditions.

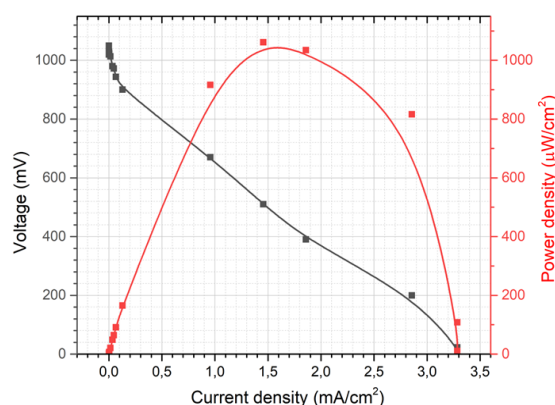


Fig. 9 – Polarization curve, derived from experimental discharge data for a VRFB with V^{4+} - V_2C MXene electrolyte solution, showing a maximum power output of $525 \mu\text{W}$ influenced by V_2C electron generation. The full color version may be accessed at <https://rrp.nipne.ro>.

4.3. ELECTROLYTE SOLUTION: V^{4+} WITH TiC_2

The voltammogram illustrates the electrochemical behavior of an experimental setup featuring a working electrode (WE) of activated carbon paper (0.7 cm^2) with V^{4+} in both anolyte and catholyte, where the anolyte contains TiC_2 MXene at a 1:9 dilution ratio, influencing the observed redox processes. The plot reveals two distinct redox couples: an anodic peak around 0.5 V and a cathodic peak around -0.5 V , likely corresponding to the V^{4+}/V^{5+} redox couple ($V^{4+} \rightarrow V^{5+} + e^-$ and $V^{5+} + e^- \rightarrow V^{4+}$), and a second set with an anodic peak near -0.5 V and a cathodic peak near -1.0 V , indicative of the V^{3+}/V^{4+} couple ($V^{4+} + e^- \rightarrow V^{3+}$ and $V^{3+} \rightarrow V^{4+} + e^-$). The 1:9 dilution of TiC_2 MXene likely enhances electrocatalytic activity and conductivity, as shown by the well-defined peaks and a current increase to 80 mA at higher potentials, suggesting improved electron transfer kinetics consistent with MXene-based electrode studies [28]. The sharp current rise beyond 1.0 V points to possible side reactions or oxygen evolution, a common occurrence with carbon-based electrodes at elevated potentials [29]. The symmetric nature of the redox peaks indicates good reversibility of the V^{4+}/V^{5+} and V^{3+}/V^{4+} couples, likely supported by MXene's presence [27], overall suggesting that the TiC_2 MXene at this dilution ratio facilitates vanadium ion redox reactions, boosting the activated carbon electrode's electrochemical performance.

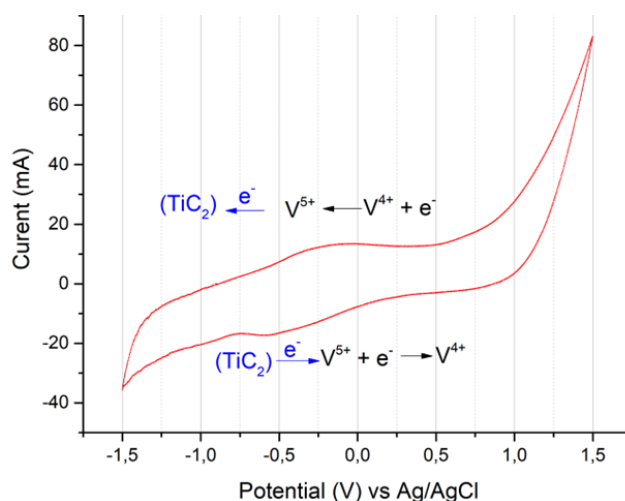


Fig. 10 – Cyclic voltammogram of V^{4+} - TiC_2 MXene electrolyte solution, scanned from -1.5 V to $+1.5 \text{ V}$ at 100 mV/s . The full color version may be accessed at <https://rrp.nipne.ro>.



Fig. 11 – VRFB battery with TiC_2 -based Mxene at a 1:9 dilution ratio, showing color stages during charging: (A) initial blue V^{4+} anolyte and catholyte, (B) obscured color transition due to the magnetic stirrer and Mxene concentration, and (C) final green V^{3+} anolyte and yellow V^{5+} catholyte, confirming successful redox reactions. The full color version may be accessed at <https://rrp.nipne.ro>.

The polarization curve in Fig.12 for the VRFB with the TiC_2 MXene - modified electrolyte demonstrates an OCV of approximately 1 V, suggesting potential inefficiencies in redox couple stability due to the additive. At a current density of 1.0 mA/cm^2 , the voltage is $\sim 0.636 \text{ V}$, reflecting activation losses comparable to V_2C MXene cell but higher than standard VRFBs. At 2.0 mA/cm^2 , the voltage drops to $\sim 0.375 \text{ V}$ indicating ohmic losses. The maximum power density of $\sim 1 \text{ mW/cm}^2$ at 1.9 mA/cm^2 highlights better high-current performance than V_2C MXene. The ohmic region ($0.5\text{--}1.5 \text{ mA/cm}^2$) shows a slope of $dV/dI \approx -0.328 \text{ V}/(\text{mA/cm}^2)$, corresponding to $R_0 \approx 0.328 \Omega \cdot \text{cm}^2$. A milder voltage drop beyond 1.9 mA/cm^2 , reaching $\sim 0.033 \text{ V}$ at 3.35 mA/cm^2 , indicates improved mass transport compared to V_2C MXene. These attributes position the TiC_2 MXene electrolyte as more suitable for high-current VRFB applications than V_2C MXene, though both are inferior to standard VRFB performance.

While the results of this experimental method yield power densities significantly lower than those of standard VRFBs; this method provides a practical platform for students to engage directly with the principles of electrochemical energy storage. By working with a simplified VRFB setup, students can explore critical concepts such as electrolyte behavior, electrode interactions, and the factors influencing battery performance.

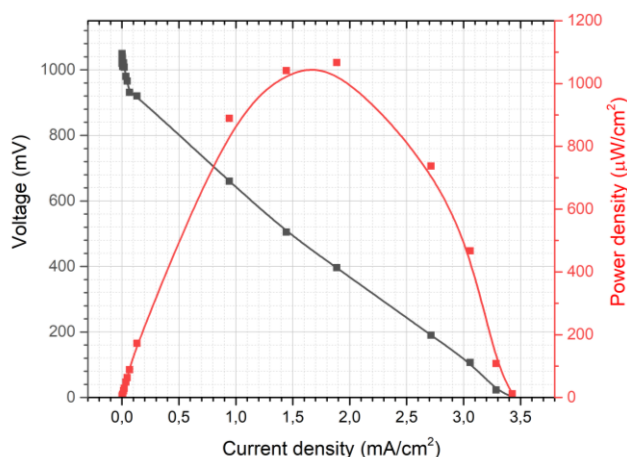


Fig. 12 – Polarization curve, derived from experimental discharge data for a VRFB with V⁴⁺-TiC₂ MXene electrolyte solution, showing a maximum power output of 520 μW with attenuated electron generation. The full color version may be accessed at <https://trp.nipne.ro>.

5. CONCLUSIONS AND PERSPECTIVES

This study presents a hands-on teaching module designed to introduce Master's students in renewable energy programs to the fundamental principles and practical applications of VRFBs. Through the preparation of vanadium-based electrolytes and electrochemical characterization using cyclic voltammetry and polarization curves, students gain direct experience with the redox processes. The experimental results confirm the reversible behavior of V⁴⁺ species and demonstrate the feasibility of using simplified laboratory setups to simulate real-world energy storage systems. This approach brings theoretical understanding of electrochemical energy storage along with laboratory skills, critical thinking, and interdisciplinary competence—qualities vital for future specialists in the renewable energy sector. Future perspectives include exploring hybrid systems that combine VRFBs with other storage technologies. Furthermore, collaboration with industry partners could provide students with exposure to current challenges and innovations in energy storage. Such initiatives contribute to the broader goal of accelerating the transition to a resilient, low-carbon energy infrastructure.

REFERENCES

1. K. Hirokazu, N. Kensaku, T. Naoto, I. Yoshikazu, M. Toshiaki, and N. Ryo, *Int. J. Hydrog. Energy* **48**, 4572–4593 (2023).
2. H. Winkler, R. Schaeffer, F. Sha, K. Riahi, and M. Meinshausen, *Nature* **534**, 631–639 (2016).

3. G. Ionescu, B. Dobrica, A. E. Balan, S. Voinea, and C. Miron, *Rom. Rep. Phys.* **77**, 903 (2025).
4. C. Radu, O. Toma, I. Antohe, C. Miron, and S. Antohe, *Rom. Rep. Phys.* **76**, 901 (2024).
5. B. Gherasim, O. Toma, C. Miron, and S. Antohe, *Rom. Rep. Phys.* **76**, 905 (2024).
6. A. Aluko and A. Knight, *IEEE Access* **11**, 13773–13793 (2023).
7. E. Sum and M. Skyllas-Kazacos, *J. Power Sources* **15**, 179–190 (1985).
8. M. Rychcik and M. Skyllas-Kazacos, *J. Power Sources* **22**, 59–67 (1988).
9. Skyllas-Kazacos, M., Kazacos, G., Poon, G. and Verseema, H., *Int. J. Energy Res.* **34**, 182–189 (2009).
10. T. Puleston, A. Clemente, R. Costa-Castelló, and M. Serra, *Batteries* **8**, (2022).
11. C. Lutz, S. Hampel, X. Ke, S. Beuermann, T. Turek, U. Kunz, A. G. Buzanich, M. Radtke, U. E. A. Fittschen, *J. Power Sources* **483**, 229176 (2021).
12. T. Haisch, H. Ji, L. Holtz, T. Struckmann, C. Weidlich, *Membranes* **11**, 232 (2021).
13. K. Ngamsai and A. Arpornwichanop, *Energy Procedia* **61**, 1642–1645 (2014).
14. K. Ngamsai and A. Arpornwichanop, *J. Power Sources* **295**, 292–298 (2015).
15. X. Z. Yuan, C. Song, A. Platt, N. Zhao, H. Wang, H. Li, K. Fatih, D. Jang, *Int. J. Energy Res.* **43**(13), 6599–6638 (2019).
16. Y. Kim, Y. Park, M. Kim, J. Lee, K. J. Kim, J. W. Choi, *Nat. Commun.* **13**(1), 2371 (2022).
17. M. Skyllas-Kazacos and M. Kazacos, *J. Power Sources* **196**(20), 8822–8827 (2011).
18. X. Ma, H. Zhang, X. Xu, S. Jiang, J. Wu, T. Chigan, and N. Chen, *ECS Meet. Abstr. MA2019-01*(3), 444 (2019).
19. Á. Cunha, J. Martins, N. Rodrigues, and F. P. Brito, *Int. J. Energy Res.* **39**, 889–918 (2015).
20. M. Skyllas-Kazacos, M. H. Chakrabarti, S. A. Hajimolana, F. S. Mjalli, and M. Saleem, *J. Electrochem. Soc.* **158**(8), R55-R79 (2011).
21. H. Agarwal, E. Roy, N. Singh, P.A.A. Klusener, R.M. Stephens and Q.T. Zhou, *Adv. Sci. (Weinh)* **11**(1) (2024).
22. N. Roznyatovskaya, J. Noack, H. Mild, M. Fühl, P. Fischer, K. Pinkwart, J. Tübke, and M. Skyllas-Kazacos, *Batteries (Basel)* **5**(1), 13 (2019).
23. G. Orijji, Y. Katayama, and T. Miura, *Electrochim. Acta* **49**, 3091–3095 (2004).
24. J. S. Lawton, S. M. Tian, D. J. Donnelly, S. P. Flanagan, T. M. Arruda, *Batteries (Basel)* **4**(3), 40 (2018).
25. A. J. Bard and L. R. Faulkner, *Electrochemical Methods: Fundamentals and Applications*, 2nd ed. Wiley, 2001.
26. B. Anasori, M. R. Lukatskaya, and Y. Gogotsi, *Nat. Rev. Mater.* **2**(2), 16098 (2017).
27. M. R. Lukatskaya, O. Mashtalir, C. E. Ren, Y. Dall'Agnese, P. Rozier, P. L. Taberna, M. Naguib, P. Simon, M. W Barsoum, Y. Gogotsi, *Science* **341**(6153), 1502–1505 (2013).
28. M. Naguib, V. N. Mochalin, M. W. Barsoum, Y. Gogotsi, *Adv. Mater.* **26**(7), 992–1005 (2014).
29. Y. Z. Pan, H. Q. Bao, N. G. Sahoo, T. F. Wu, L. Li, *Adv. Funct. Mater.* **21**(14), 2754–2763 (2011).